Fluid-Structure-Interaction Applying a Ghost-Cell Immersed Boundary Method

Eike Hylla and Frank Thiele

Abstract. An established *Immersed Boundary* flow solver has been coupled with a newly developed structural solver employing the Finite Element Method. The coupling algorithm is presented as well as some essential details of both solvers. The structural solver is validated for different test cases. The approach is applied to the flow past an elastic cylinder.

1 Introduction

One difficulty of Fluid-Structure-Interaction (FSI) is the changing of geometries. In case of a body conformal discretisation, a change of the body shape implicates modifications of the grid. These are commonly realised by grid deformation techniques often involving additional coasts, while they are limited to moderate deformations. In this situation non body conformal grid approaches become advantageous. The IB-Method [1] is a suitable approach for the simulation of flows in complex and moving geometries. The governing equations can be discretised on a Cartesian grid and the boundary conditions are applied considering an additional surface mesh representing the geometry. Utilising separate grids for the computation and the imposition of the boundary conditions allows for an exchange of the surface description during the simulation. This conveniently enables the consideration of moving or deforming geometries without being restricted to grid deformation techniques. The methodology mentioned above is successfully employed for different cases with a prescribed motion or deformation, e.g. an oscillating rectangular prism [2] or the respiratory flow within dynamic airway geometries [3]. In the present paper the aspect of an *interaction* between the fluid and an immersed structure will be discussed. Section 2 gives an overview over the flow solver with respect to FSI.

Eike Hylla · Frank Thiele
Berlin Institute of Technology, Chair of Fluid Mechanics and Engineering Acoustics, Müller-Breslau-Str. 12, 10623 Berlin, Germany
e-mail: eike.hylla@cfd.tu-berlin.de

A. Dillmann et al. (Eds.): *New Results in Numer. & Exp. Fluid Mech.*, NNFM 121, pp. 473–480.
DOI: 10.1007/978-3-642-35680-3_56

The triangular surface discretisation of the flow solver is directly used for the structural simulation. An Finite Element Method (FEM) solver, employing shell elements representing thin structures, has been derived, implemented and validated (see section 3). Both solvers are subsequently coupled by an iterative procedure (section 4) in order to simulate problems of thin elastic structures interacting with the flow field. The steady and laminar flow past a elastic circular cylinder is an appropriate first test case for the developed approach (section 5).

2 IB Flow Solver

The governing equations of the fluid mechanical part are the law of mass conservation for the incompressible case (1) and the equations of momentum balance (2):

$$\nabla \cdot \mathbf{u} = 0, \tag{1}$$

$$\frac{\partial \mathbf{u}}{\partial t} + (\mathbf{u} \cdot \nabla)\,\mathbf{u} + \frac{1}{\rho}\nabla p - \nu \nabla^2 \mathbf{u} = 0, \tag{2}$$

where $\mathbf{u}$, p, ρ, ν and t are the velocities, pressure, density, kinematic viscosity and time, respectively. The Finite Volume discretisation of the flow solver is of second order accuracy in space and time. The state variables are calculated successively using the SIMPLE algorithm combining pressure and velocity fields. A non body conformal Cartesian discretisation is used in which the boundary conditions are imposed by the IB-method. There are different ways of imposing the boundary conditions at the immersed surface [4]. In this work a *Ghost-Cell method* [5] is used.

2.1 Moving Wall Boundaries

The IB surface separates the computational domain into fluid and solid sections. Therefore an identification and marking procedure is necessary to distinguish between fluid and non-fluid regions prior to the simulation. At an IB wall the velocities of the ghost-cells are interpolated to fulfil the no slip condition. In the case of a moving wall the surface is exchanged after each time step, followed by the identification and marking process again. The velocity $\mathbf{u}_{\mathrm{IB}}$ is currently approximated by a backward difference scheme of first-order accuracy:

$$\mathbf{u}_{\mathrm{IB}} = \frac{\mathrm{d}\mathbf{x}}{\mathrm{d}t} \approx \frac{\mathbf{x}(t) - \mathbf{x}(t-\Delta t)}{\Delta t}\,, \tag{3}$$

where $\mathbf{x}$ is the vector to each point of the surface grid. Due to the modification of the surface mesh two effects can occur: fluid cells may become non-fluid cells and vice versa. In the first case the stored variables of the now non-fluid cells are simply neglected. In the second case where a non-fluid cell has changed to a fluid cell an appropriate initialisation is needful. The velocity and pressure values for the mentioned cells are gained from the nearest point of the IB. The space convervation law [6] is not fulfilled.

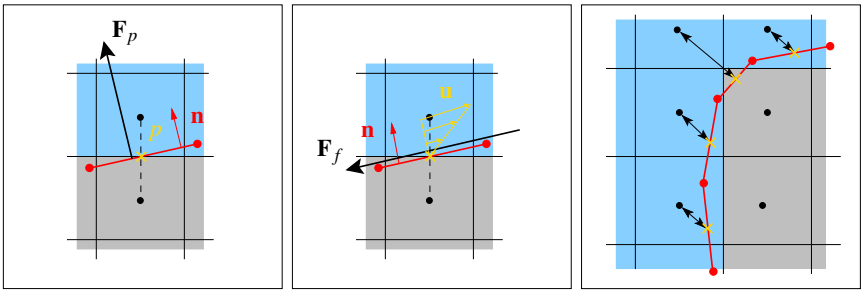

Fig. 1 Calculation of forces at the IB: due to pressure (*left*) and friction (*middle*); nearest fluid cell associated with each triangle element (*right*). Centre of Cartesian cell (•), position of stored values (x), IB triangle (•—•), fluid region (■), non-fluid region (■).

2.2 Calculation of Forces

The forces of the fluid at the immersed body $\mathbf{F}_{\text{fluid}}$ contains forces caused by the pressure $\mathbf{F}_p$ and forces due to the wall friction $\mathbf{F}_f$:

$$\mathbf{F}_{\text{fluid}} = \mathbf{F}_p + \mathbf{F}_f = p A_\triangle \mathbf{n} - \tau_w A_\triangle \mathbf{n}. \tag{4}$$

The forces are determined for each element of the surface grid located in the triangle centre. The pressure at each IB triangle, its normal vector $\mathbf{n}$ and the area $A_\triangle$ have to be known to calculate $\mathbf{F}_p$ (fig. 1 *left*). The wall shear stresses (τ_w) determine the friction forces $\mathbf{F}_f$ (fig. 1 *middle*). To compute the shear stresses, it is necessary to obtain the velocity gradient in wall normal direction. As the surface elements have an arbitrary orientation with respect to the Cartesian grid, some extra work is required: For each surface element the nearest fluid cell (ideally in normal direction) has to be found (fig. 1 *right*). This kind of point to point search is done once for a certain surface configuration. Based on the velocities at the IB and the located nearest cell a gradient is computed, which is then corrected in wall normal direction.

3 FEM Structural Solver

The implemented FEM structural solver is based on the theory of linear elasticity. Within the process of development, different element types were integrated, resulting in a three-dimensional description of shell elements (see section 3.1). Independently from the type of element, the FEM discretisation leads to an equation:

$$\mathbf{K} \times \mathbf{u}_s = \mathbf{f}. \tag{5}$$

$\mathbf{K}$ is the total stiffness matrix, $\mathbf{u}_s$ the vector of deflections (and rotations) and $\mathbf{f}$ containing the loads (forces and moments). The matrix $\mathbf{K}$ is sparse symmetric and stored in compressed row storage (CRS) format. The Dirichlet boundary condition of a zero deflection is realised by dropping corresponding entries of the matrix. The

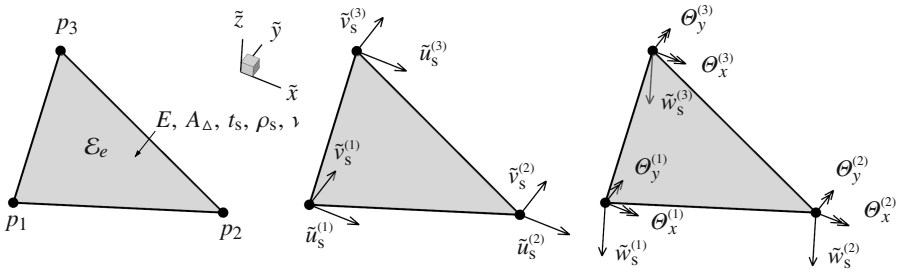

Fig. 2 Triangle element $\mathcal{E}_e$, defined by the nodes p_n (*left*); element with in-plane deformations $\tilde{u}_s^{(n)}, \tilde{v}_s^{(n)}$ (*middle*); plate bending element with deformations $\tilde{w}_s^{(n)}$ and rotations $\Theta_x^{(n)}$, $\Theta_y^{(n)}$ (*right*)

equation system (5) is solved by a BiCGSTAB solver with diagonal preconditioning [7].

3.1 Triangle Shell Elements

Shell elements are 2d elements which can represent in-plane deformations and deflections normal to its orientation. They are commonly applied for modelling thin structures. In the current implementation they are represented by triangles, defined by its three nodes p_n. Each element $\mathcal{E}_e$ is formulated in local coordinates $\tilde{x}, \tilde{y}, \tilde{z}$ (see fig. 2 *left*). The mechanical properties are the modulus of elasticity E, the Poisson ratio ν_s, the density ρ_s, the thickness t_s and the area $A_\triangle$ of the triangle. The stiffness $\tilde{\mathbf{K}}_\mathrm{e}^\mathrm{shell}$ of the shell element can be derived by combining the stiffness relations of the plane element $\tilde{\mathbf{K}}_\mathrm{e}^\mathrm{plane}$ and plate element $\tilde{\mathbf{K}}_\mathrm{e}^\mathrm{plate}$ (see fig. 2 *middle* and *right*). A conventional linear element [8] is chosen to represent the in-plane deformations $\tilde{u}_\mathrm{s}$, $\tilde{v}_\mathrm{s}$. A plate bending element by Specht [9] is added to consider the normal displacements $\tilde{w}_\mathrm{s}$ and the rotations Θ_x and Θ_y. The stiffness matrix for each element is derived in the local coordinate system (fig. 2 *left*). Usually the triangles are oriented arbitrarily in space, which makes a transformation from the local to the global coordinate system necessary:

$$\mathbf{K}_\mathrm{e} = \mathbf{T}^\mathrm{T}\, \tilde{\mathbf{K}}_\mathrm{e}\, \mathbf{T}, \tag{6}$$

in which $\mathbf{T}$ is a transformation matrix on the basis of the direction cosine [8]. The resulting element stiffness matrices are then assembled into the total stiffness matrix $\mathbf{K}$.

3.2 Validation

The novel implemented approach has been validated for several test cases: first for elements in the local and later for elements in the global coordinate system. The results are exactly matching apart from some slight numerical differences caused

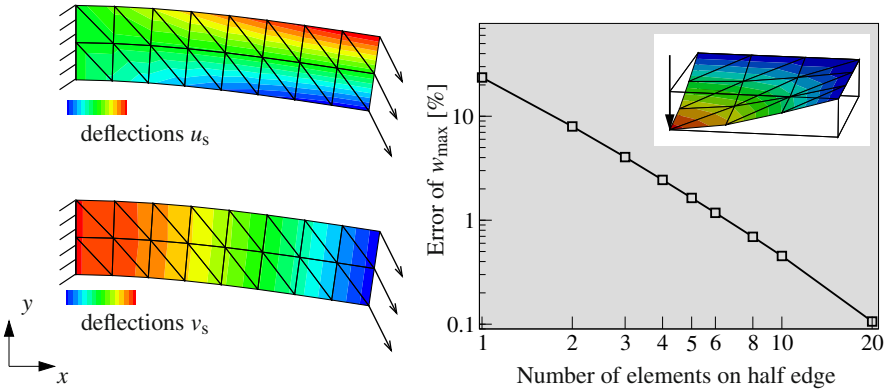

Fig. 3 Beam test case of in-plane deformations (*left*); convergence of the plate element (*right*)

by the coordinate transformation. The shell element is also able to represent pure in-plane and pure bending deformations, shown in figure 3. The results for a cantilever beam (fig. 3 *left*) completely agree with the results published in [10]. A fully supported square plate (fig. 3 *right*) with a single vertical force in the centre is a standard test case for the verification and validation of plate elements. In a convergence test the numerical solution can be compared to the analytical solution of the problem [11]. The results of this test fully agree with the data published in [10].

4 Coupling Algorithm

The two introduced methods are loosely coupled by an iterative procedure similar to the one published in [12]. Figure 4 presents a flow chart of the coupling procedure, which currently works well for steady cases. The FSI iteration ($\mathcal{F}$) can be summarised as follows: after a certain number of iterations in the flow solver the loads induced by the fluid $\mathbf{F}_{\text{fluid}}$ are transferred[1] to the FE solver and the solver is executed. The resulting deflections are added to the geometry and the CFD computation is continued, after the identification procedure has finished. For the following FSI iteration ($\mathcal{F}+1$) the procedure is repeated. The currently computed loads are applied to the undeflected geometry respectively. To control the FSI iteration a residual based on the Euclidean norm of the force differences (for each node n) is generated:

$$\mathcal{R}_{\text{FSI}} = \left\| \mathbf{F}_{\mathcal{F}+1} - \mathbf{F}_{\mathcal{F}} \right\| = \sum_{n=1}^{n_{\max}} \sqrt{\left(\mathbf{F}^n_{\mathcal{F}+1} - \mathbf{F}^n_{\mathcal{F}} \right)^2} \,. \tag{7}$$

[1] The surface mesh of the flow computation is directly utilised for the FEM simulation. The force vectors of adjacent triangle elements are averaged to the nodes. These forces are also causing bending moments [10], which are currently neglected as a first approach.

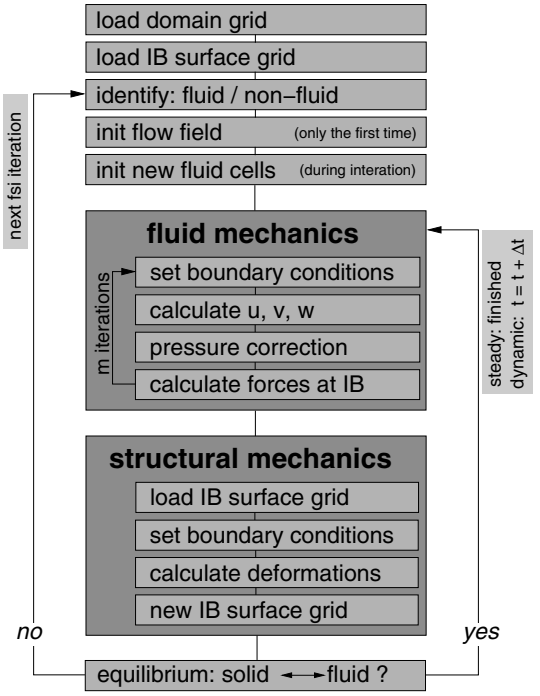

Fig. 4 Flow chart of the iterative coupling algorithm

If the residual is smaller than a certain minimum value $\mathcal{R}_{\text{FSI}} < \mathcal{R}_{\text{min}}$ the FSI iteration stops. The allowed maximum iteration number $\mathcal{F}_{\text{max}}$ and the minimum residual $\mathcal{R}_{\text{min}}$ have to be adjusted manually.

5 Application: Flow Around an Elastic Cylinder

The coupled system has been applied to the steady laminar [13] flow ($\text{Re}_d = 20$) past an elastic cylinder. The cylinder ($h/d = 2$) is fully supported at the upper and lower face. For the FSI iteration the flow field is initialised with the steady solution past a rigid cylinder. The surface grid consists of $\approx 9,500$ triangles and the volume grid of $\approx 500,000$ Cartesian cells respectively. The properties of the cylinder (E, ν_s, ρ_s, t_s) are chosen in relation to the fluid properties (ρ, ν, $\mathbf{u}_\infty$) such that moderate deformations occur (compare fig. 6).

5.1 Results and Discussion

Within about 10 FSI iteration steps the FSI convergence reaches a constant level of $\mathcal{R}_{\text{FSI}} \approx 4.0 \cdot 10^{-4}$ (see fig. 5 *left*). No further changes of the flow field and of the deflected geometry are observed for an increasing iteration number. At this

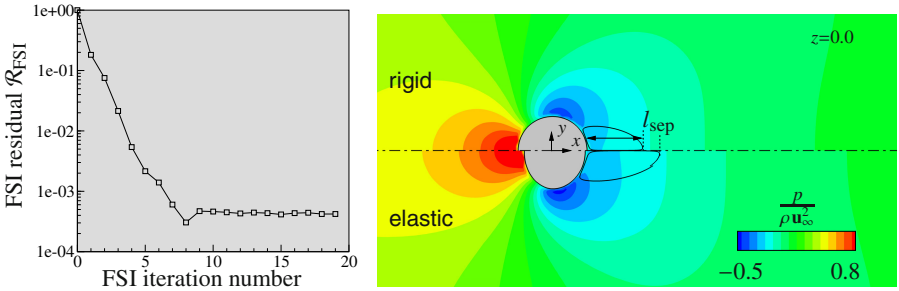

Fig. 5 FSI convergence (*left*); comparison of rigid and elastic cylinder at Re = 20 (*right*)

stage an equilibrium between the two solutions is reached. The flow regime of around the deflected geometry remains steady and laminar. Figure 5 *right* depicts a comparison of the flow past the rigid and the elastic cylinder. Under the forces of the fluid (mainly determined by the pressure) the cylinder flattens at the front and increases its cross section in the y-direction. The new shape of the deformed cylinder is displayed in fig. 6. The flattened front extends the high pressure region whereas the enlargement in y-direction causes a higher amount of pressure drop at the side regions. For a cylinder flow at $\mathrm{Re}_d = 20$ the separation length is equal to the diameter $l_{\mathrm{sep}} \approx d$. Due to the magnification of the cylinder normal to the mean flow direction the Reynolds number increases, which consistently leads to an enlargement of the separation length (compare fig. 5).

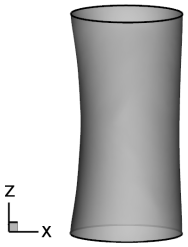

Fig. 6 Deformed cylinder

6 Conclusions and Outlook

In this paper the coupling of an IB flow solver with an FEM solver on the basis of shell elements has been demonstrated. There are however some limitations that should not be rejected: The IB-Method is restricted to moderate Reynolds numbers because of insufficient near wall grid resolution by the Cartesian cells. The FEM implementation is currently based on the linear theory, which is usually only valid for small deformations of a linearly elastic material. Furthermore the test configuration is far away from typical engineering problems. Nevertheless we successfully demonstrated a convenient way of combining both solvers in which only the interacting forces have to be transferred. The surface grid of the flow simulation is directly considered in the FEM solver. However to simulate more realistic problems further development of the structural solver and an enhancement to the non-linear theory is necessary. Instead of that an existing solver (commercial or open source) could be engaged.

References

1. Peskin, C.S.: The immersed boundary method. Acta Numerica, 479–512 (2002)
2. Hylla, E., Frederich, O., Mauß, J., Thiele, F.: Application of the Immersed Boundary Method for the Simulation of Incompressible Flows in Complex and Moving Geometries. In: Dillmann, A., Heller, G., Klaas, M., Kreplin, H.-P., Nitsche, W., Schröder, W. (eds.) New Results in Numerical and Experimental Fluid Mechanics VII. NNFM, vol. 112, pp. 135–142. Springer, Heidelberg (2010)
3. Hylla, E., Frederich, O., Thiele, F., Puderbach, M., Ley-Zaporozhan, J., Kauczor, H.-U., Wang, X., Meinzer, H.-P., Wegner, I.: Analysis of the Flow in Dynamically Changing Central Airways. In: Klaas, M., Koch, E., Schröder, W. (eds.) Fundamental Medical and Engineering Investigations on Protective Artificial Respiration. NNFM, vol. 116, pp. 33–48. Springer, Heidelberg (2011)
4. Mittal, R., Iaccarino, G.: Immersed boundary methods. Annual Review of Fluid Mechanics 37, 239–261 (2005)
5. Tseng, Y.-H., Ferziger, J.H.: A ghost-cell immersed boundary method for flow in complex geometry. Journal of Computational Physics 192(2), 593–623 (2003)
6. Demirdžić, I., Perić, M.: Space conservation law in finite volume calculations of fluid flow. International Journal for Numerical Methods in Fluids 8(9), 1037–1050 (1988)
7. Saad, Y.: Iterative Methods for Sparse Linear Systems. SIAM (2003)
8. Zienkiewicz, O.C., Taylor, R.L.: The Finite Element Method for Solid and Structural Mechanics. Elsevier Butterworth-Heinemann (2005)
9. Specht, B.: Modified Shape Functions for the Three-Node Plate Bending Element Passing the Patch Test. International Journal for Numerical Methods in Engineering 26(3), 705–717 (1988)
10. Steinke, P.: Finite-Elemente-Methode. Springer (2007)
11. Timoshenko, S., Woinowsky-Krieger, S.: Theory of Plates and Shells. McGraw-Hill (1959)
12. Yigit, S., Heck, M., Sternel, D.C., Schäfer, M.: Efficiency of Fluid-Structure Interaction Simulations with Adaptive Underrelaxation and Multigrid Acceleration. International Journal of Multiphysics 1(1), 85–98 (2007)
13. Zdravkovich, M.M.: Flow Around Circular Cylinders. Fundamentals, vol. 1. Oxford Science Publications (1997)